**TITLE PAGE**

***Title:***

# Unraveling Vulnerabilities in Endocrine Therapy-Resistant HER2+/ER+ Breast Cancer

***Authors:***

Shaymaa Bahnassy[1], Hillary Stires[2], Lu Jin[1], Stanley Tam[1], Dua Mobin[1], Manasi Balachandran[3], Mircea Podar[4], Matthew D. McCoy[1], Robert A. Beckman[5], Rebecca B. Riggins[1*]

***Affiliations:***

[1]Department of Oncology, Lombardi Comprehensive Cancer Center, Georgetown University, Washington, DC.

[2]Friends of Cancer Research, Washington, DC.

[3]Department of Medicine, University of Tennessee Medical Center, Knoxville, TN.

[4]Oak Ridge National Laboratory, Oak Ridge, TN.

[5]Departments of Oncology and of Biostatistics, Bioinformatics, and Biomathematics, Lombardi Comprehensive Cancer Center and Innovation Center for Biomedical Informatics, Georgetown University Medical Center, Washington, DC

***Running title:*** Characterizing Endocrine-therapy resistance HER2+/ER+ Breast Cancer

***Keywords:*** Breast cancer; Endocrine resistance; HER2+/ER+; Human epidermal growth factor receptor 2

***Corresponding Author:*** Rebecca B. Riggins, 3970 Reservoir Rd NW, E412 Research Bldg, Washington, DC 20057, email rbr7@georgetown.edu

***Funding:*** This work was funded by the Department of Defense (DoD) Breast Cancer Research Program awards W81XWH-20-1-0759 and W81XWH-20-1-0760 (to RBR and RAB, respectively), the Oak Ridge National Laboratory Director's R&D fund (to MP and RAB), and philanthropy support from Lombardi Women at Georgetown Lombardi's Nina Hyde Center for Breast Cancer Research (to RBR). Fellowship support for HS and ST was provided by the Tumor Biology Training Grant T32 CA009686 (principal investigator (PI): Dr. Anna T. Riegel). DM received support from the Georgetown Regents Scholars Program. Technical services were provided by the GUMC Genomics and Epigenomics, Microscopy and Imaging, and Tissue Culture Shared Resources, which are supported, in part, by NIH/NCI Cancer Center Support Grant P30 CA051008 (PI: Dr. Louis M. Weiner). The content of this article is the sole responsibility of the authors and does not represent the official views of the DoD or NIH.

***Disclosures:*** SB, HS, LJ, ST, DM, MB, MP, and MDM have nothing to declare. RAB consults for AstraZeneca LP and Boehringer Ingelheim, and is the Chief Scientific Officer and Managing Member of Onco-Mind, LLC, which owns patents related to cancer precision medicine. RBR is an Associate Editor for the Journal of the Endocrine Society.

## ABSTRACT

### Background

Breast tumors overexpressing human epidermal growth factor receptor (HER2) confer intrinsic resistance to endocrine therapy (ET), and patients with HER2/ estrogen receptor-positive (HER2+/HR+) breast cancer (BCa) are less responsive to ET than HER2-/ER+. However, real-world evidence reveals that a large subset of HER2+/ER+ patients receive ET as monotherapy, positioning this treatment pattern as a clinical challenge. In the present study, we developed and characterized two distinct *in vitro* models of ET-resistant (ETR) HER2+/ER+ BCa to identify possible therapeutic vulnerabilities.

### Methods

To mimic ETR to aromatase inhibitors (AI), we developed two long-term estrogen-deprived (LTED) cell lines from BT-474 (BT474) and MDA-MB-361 (MM361). Growth assays, PAM50 molecular subtyping, genomic and transcriptomic analyses, followed by validation and functional studies, were used to identify targetable differences between ET-responsive parental and ETR-LTED HER2+/ER+ cells.

### Results

Compared to their parental cells, MM361 LTEDs grew faster, lost ER, and increased HER2 expression, whereas BT474 LTEDs grew slower and maintained ER and HER2 expression. Both LTED variants had reduced responsiveness to fulvestrant. Whole-genome sequencing of the more aggressive MM361 LTED model system identified exonic mutations in genes encoding transcription factors and chromatin modifiers. Single-cell RNA sequencing demonstrated a shift towards non-luminal phenotypes, and revealed metabolic remodeling of MM361 LTEDs, with upregulated lipid metabolism and antioxidant genes associated with ferroptosis, including

69 *GPX4*. Combining the GPX4 inhibitor RSL3 with anti-HER2 agents induced significant cell death
70 in both the MM361 and BT474 LTEDs.
71
72 **Conclusions**
73 The BT474 and MM361 AI-resistant models capture distinct phenotypes of HER2+/ER+ BCa
74 and identify altered lipid metabolism and ferroptosis remodeling as vulnerabilities of this type of
75 ETR BCa.

## INTRODUCTION

Globally, breast cancer (BCa) remains the leading cause of cancer-related mortality in women (1). Human epidermal growth factor receptor positive/ hormone receptor positive (HER2+/HR+) tumors account for approximately 10% of all BCa cases and 60% of HER2+ tumors (2). HER2+/ estrogen receptor positive (ER+) and HER2+/ER- BCa have distinct biology and are proposed as two distinct disease subtypes (3,4). Prior and recent studies reported favorable prognosis and overall survival (OS) as well as lower-grade tumors in HER2+/ER+ BCa compared to HER2+/ER- BCa patients (5-8). However, HER2+/ER+ BCa has low response rates to anti-HER2 therapy compared to HER2+/ER- tumors (9,10), have a limited antiproliferative response to endocrine therapy (ET), and are at a higher risk of recurrence (2,10,11).

Concurrent blockade of both HER2 and ER pathways in patients with advanced/metastatic HER2+/ER+ BCa is becoming increasingly evident as an effective treatment strategy. In clinical trials, postmenopausal women receiving combinations of ET plus anti-HER2 as first-line therapy showed improvements in progression-free survival (PFS) and/or other clinical benefits (12-14). Likewise, a retrospective study of the national cancer database showed the highest 5-year OS among those receiving this combination therapy vs. ET alone, chemotherapy alone or anti-HER2 + chemotherapy (15). Unfortunately, outside of clinical trials a large subset (36.7-60%) of HER2+/ER+ patients receive hormonal treatment as a monotherapy (15,16). Although current guidelines recommend anti-HER2 agents (trastuzumab + pertuzumab; TP) plus chemotherapy as first-line standard of care for advanced HER2+ disease irrespective of HR status, endocrine monotherapy remains an option for selected HER2+/ER+ patients that have low disease burden or intolerance to chemotherapy (17,18). Moreover, antibody-based anti-HER2 therapy is mainly given to patients with primary HER2+/ER+ BCa for one year, while ET is usually given longer (at least five years) (2). Thus, residual HER2+/ER+ disease after surgery, not subjected to anti-HER2 therapy, remains at high risk of incomplete response or resistance to prolonged ET.

A shorter time to recurrence in patients with HER2+ disease, compared to HER2-, treated with single-agent ET as tamoxifen or anastrozole was reported (19). Likewise, compelling evidence from preclinical and clinical data strongly suggests that HER2 overexpression confers intrinsic resistance to ET and that HER2+/ER+ BCa are less responsive to ET than HER2-/ER+ tumors (2,10,20). Multiple studies have further established that bi-directional crosstalk between ER and HER2 signaling pathways mediates resistance to ET (21-23). While acquired ET resistance is extensively studied in HER2-/ER+ BCa, preclinical models of HER2+/ER+ BCa that have acquired resistance to ET are lacking. Existing models of resistance have been generated by genetic manipulations of ER and/or HER2, for example (24,25).

Collectively, there is an unmet need to develop, characterize and study therapeutic responses of ET-resistant (ETR) HER2+/ER+ models to HER2- and other ER-directed therapies. In this study, we establish ETR variants through long-term estrogen deprivation (LTED) to mimic resistance to aromatase inhibitors (AI) from two HER2+/ER+ BCa cell lines (BT474 and MDA-MB-361, (26,27)). To identify therapeutic vulnerabilities between AI-responsive-parentals and ETR-LTEDs of HER2+/ER+ BCa cell lines, we performed growth assays, PAM50 molecular subtyping, genomic and transcriptomic analyses. Our data shows that the BT474 and MM361 ETR models capture distinct phenotypes of HER2+/ER+ BCa and highlight altered lipid metabolism and ferroptosis remodeling as features of this ETR BCa.

## METHODS

### Treatments, Cell Lines, and Cell Culture

Trastuzumab and pertuzumab were obtained from Genentech, SYTOX green (S7020) and Hoechst 33342 (H1399) from ThermoFisher, fulvestrant (S1191) from Selleck Chemicals, β-estradiol (E8875) from Sigma Aldrich and RSL3 (HY-100218A) from MedChemExpress.

MDA-MB-361 (MM361; RRID:CVCL_0620) and BT-474 (BT474; RRID:CVCL_0179) human breast carcinoma cell lines were obtained from the Tissue Culture and Biobanking Shared Resource at Lombardi Comprehensive Cancer Center and were routinely checked for *Mycoplasma* contamination. Both cell lines were cultured in improved Minimum Essential Medium (IMEM; Gibco) media supplemented with 10% FBS at 37°C in a humidified atmosphere containing 5% $CO_2$. We generated two LTED variants A and B cells from their corresponding parental cell lines by chronically passaging parental cell lines in phenol red-free IMEM media (Gibco) supplemented with 10% charcoal-stripped bovine serum (CSS; Vita Scientific) for over six months. After developing resistance, the derived cells were used and continuously cultivated in 10% CSS phenol red-free IMEM.

**Growth Assays**

Differences in growth kinetics between parental and corresponding LTEDs were evaluated by the trypan blue exclusion assay. Cells were seeded at a density of 100,000 cells/well in 24-well plates. After trypsinization and staining with trypan blue, live cell counts using the Countess II Automated Cell Counter (ThermoFisher Scientific) were recorded on days 0 (24 h), 2, 4, 6, 8, and 10 from cell seed.

For crystal violet assays, parental and LTED cells were seeded in 96-well plates at 5,000 cells/well. Forty-eight hours later, cells were subjected to indicated treatments for six additional days. Treatments were replenished three days after treatment onset. At the end of the experiments, cells were stained with 0.5% crystal violet in 25% methanol. Once plates were dried, the stain was resolubilized with citrate buffer, and absorbance measurements were obtained from the ELx808 plate reader (BioTek).

**Cell Death Quantification**

Cells were seeded in 24-well plates at a cell density of 150,000 cells/well, incubated overnight, then subjected to treatments as indicated. After 72□h of treatments, cells were stained with both Hoechst 33342 (0.1 µg/mL) to monitor total cell number, and Sytox green (5 µM) to monitor dead cells. Images were acquired using the Olympus IX71 microscope and subsequently analyzed by Image J. Percentage cell death was calculated as Sytox green cell number over total cell number.

**Western Blot Analysis**

Whole-cell protein extracts were denatured, resolved on NuPAGE 4-12% Bis-Tris gels (ThermoFisher), and either transferred onto nitrocellulose membranes using iBlot 2 dry transfer apparatus (ThermoFisher) or PVDF membranes using the BioRad wet transfer apparatus. After blocking, blots were probed overnight, and the following primary antibodies were used: ER (Cell Signaling Technology Cat# 8644, RRID:AB_2617128), EGFR (Cell Signaling Technology Cat# 2232, RRID:AB_331707), HER2 (Cell Signaling Technology Cat# 2242, RRID:AB_331015), pHER2 (Cell Signaling Technology Cat# 2241, RRID:AB_2099407), HER3 (Cell Signaling Technology Cat# 12708, RRID:AB_2721919), HER4 (Cell Signaling Technology Cat# 4795, RRID:AB_2099883) , AKT (Cell Signaling Technology Cat# 4691, RRID:AB_915783), pAKT (Cell Signaling Technology Cat# 9271, RRID:AB_329825), β-actin (Cell Signaling Technology Cat# 3700, RRID:AB_2242334), vinculin (Cell Signaling Technology Cat# 13901, RRID:AB_2728768), 4-HNE (Abcam Cat # ab46545, RRID: AB_722490), GPX4 (Abcam Cat# ab125066, RRID:AB_10973901), MDA (Thermo Fisher Scientific Cat# MA5-27559, RRID:AB_2735264) and GAPDH (Proteintech Cat# 60004-1-Ig, RRID:AB_2107436). After one hour of incubation with secondary antibody (either anti-mouse (Cell Signaling Technology Cat# 7076, RRID:AB_330924) or -rabbit (Cell Signaling Technology Cat# 7074, RRID:AB_2099233))

and washes, antigen-antibody complexes were detected by the chemiluminescence WesternBright ECL Detection Reagent (Advansta) and imaged using the Amersham Imager 600 (GE Healthcare Life Sciences).

**Real-time PCR (qRT-PCR)**

Total RNA of biological triplicates was extracted from cells using the PureLink RNA Mini Kit (ThermoFisher) and converted to cDNA with iScript cDNA Synthesis Kit (BioRad) according to manufacturer's instructions. Expression of target genes with specific primers (sequences listed in Table S1 (28); synthesized by IDT) was measured by RT-qPCR using the iTaq Universal SYBR Green Supermix (BioRad) and QuantStudio 12K Flex Real-Time PCR System (ThermoFisher). Data were normalized to the ß-actin housekeeping gene and analyzed by the ΔΔCT method.

**Single-Cell RNA Sequencing (scRNAseq)**

The scRNAseq was performed using the Drop-seq approach described by Macosko *et al*. (29) with updates and detailed workflow from the McCarroll lab at Harvard Medical School (https://mccarrolllab.org/dropseq/). To generate the droplet emulsion and cell encapsulation we used a Dolomite-Bio µEncapsulation system (Dolomite-Bio) according to manufacturer's instructions. Barcoded beads were purchased from Chemgenes, as specified by (29). Briefly, trypsinized MM361 parental and LTED cells were washed, and resuspended in PBS-0.01% BSA. The single-cell suspension, bead suspension, and the droplet generation oil were loaded into their respective containers and connected via high precision pumps to the scRNA chip as part of the µEncapsulation system. The flow rates were adjusted so that each droplet generated encapsulated one bead and one cell and monitored under the system's high speed digital microscope. Droplets were collected, and a small aliquot was examined microscopically to

ensure uniformity of bead size and occupancy. The beads were washed and used for reverse transcription/cDNA synthesis and PCR according to the drop-seq workflow. The PCR products were purified, pooled, and quantified in a BioAnalyzer High Sensitivity Chip (Agilent). Sequencing libraries were prepared using the Nextera XT DNA sample prep kit (Illumina Inc) following manufacturer's protocol. The libraries were purified, quantified, and sequenced by GenWiz on an Illumina High-Seq instrument using 2x150 nt reads.

Raw data was imported into the Seurat R package (30). All cells with unique feature counts between 200 and 2500 and a percentage of mitochondrial reads less than 5% were selected for further analysis. After scaling, dimensional reduction, and cell type specific marker identification with default parameters, we discovered 7 different clusters among LTED and parental cell lines. Differentially expressed genes ($p < 0.05$) were calculated between all three experimental groups. A combined LTED and parental cell lines UMAP was generated with 10 PC and 0.5 resolution. We also performed PAM50 molecular classification using genefu R package (31) at single-cell resolution; a treatment split UMAP was generated with the same settings.

**Gene Set Enrichment Assay (GSEA)**

Differentially expressed genes were matched against the REACTOME signature from the Human Molecular Signature Database (MSigDB) using the GSEA portal (http://software.broadinstitute.org/gsea/index.jsp) (32), with false discovery rate (FDR) q-values <0.05. Top 20 enriched pathways and their corresponding - log (p-value) were graphed.

**Whole Genome Sequencing (WGS)**

DNA was extracted from cells using the DNeasy Blood and Tissue Kit (Qiagen) according to manufacturer's instructions. The Genomics and Epigenomics Shared Resource (GESR) at Georgetown University Medical Center performed the WGS. Paired-end, indexed libraries for

human WGS were constructed from 1.0 µg of gDNA using the TruSeq DNA PCR-Free Library Prep Kit (Illumina) according to the manufacturer's instructions. Briefly, DNA was fragmented using a Covaris M220 Focused-ultrasonicator (Covaris) using settings for a 350-bp insert size. Library quality was assessed with a BioAnalyzer 2100 using the High Sensitivity DNA kit (Agilent Technologies). The libraries were quantified using the Kapa Library Quantification Kit Illumina Platforms (Kapa Biosystems). The denatured and diluted libraries were sequenced on a NextSeq 550 System (Illumina) using v2.5 High Output 300 cycle kit with 1% PhiX to an average sequencing depth of 50x coverage.

The quality of raw sequence data (fastq or fasq.gz files) was checked by FastQC v0.11.9 (33), and Cutadapt v3.5 was used for adapter trimming of raw data (34). After trimming, reads with low quality (quality score < 33, error rate > 10%) and lengths less than 25 bp were eliminated. Processed reads were then aligned to GRCh38 reference sequence using the bwa v0.7.17 paired-end mode (35). Mutation detection was conducted in Genome Analysis Toolkit (GATK) v4.1.9.0 (36) following the best practice for variant calling workflow. SigProfiler (37) on COSMIC Mutational Signatures version 3.2 was used to classify single base substitution (SBS) in WGS data.

**Statistical Analysis**

All results are expressed as mean ± SEM. Prism 9 (GraphPad Software) was used for data analysis. Unless otherwise noted, one-way ANOVA followed by Tukey's or Dunnett's multiple comparison tests were employed to evaluate statistical significance between groups and *p*-values < 0.05 were considered statistically significant.

**RESULTS**

***Patients of the HER2+ BCa subtype expressing high levels of ESR1 exhibit lower risk for metastasis***

We analyzed a publicly available database to evaluate patients' survival rates of HER2+ BCa stratified by their HR status. Regardless of HR status, five-year survival rates from the SEER database for patients with HER2+ BCa decrease with disease progression and are the lowest for late (distant)-stage HER2+ BCa (**Fig. 1A**). Next, we specifically focused on ER and compared survival rates of HER2+ BCa patients as stratified by high and low estrogen receptor alpha gene (*ESR1*) expression. Ten-year survival data from the Kaplan-Meier Plotter database (38) show no difference in overall survival (OS) and relapse-free survival (RFS) between patients expressing high or low levels of *ESR1* (**Fig. 1B** and **1C,** respectively). On the contrary, patients expressing high levels of *ESR1* show higher probability for distant metastasis-free survival (DMFS) (logrank $P$ = 0.035, **Fig. 1D**), and thus lower risk for metastasis. This lower susceptibility for metastasis suggests correlation of high ER expression with better prognosis within the advanced setting of HER2+ BCa disease.

***Growth patterns and responses to HER2- and ER-targeted therapies of HER2+/ER+ LTEDs differ from their parental counterparts***

To mimic acquired ETR to AI, we generated two LTED variants (A and B) from each of the two HER2-amplified, HER2+/ER+ BCa cell lines (**Fig. 2A** and **2B**): BT474 and MM361 (26,27). We first compared proliferation behaviors of LTEDs versus their corresponding parental cell lines grown in media supplemented with either FBS or CSS (CSS represents short-term hormone starvation). BT474 LTEDs had significantly lower growth rates than their respective parentals grown in FBS media but were not different from parentals in CSS media (**Fig. 2C** left panel). On the other hand, MM361 LTEDs grew faster than parentals in CSS and FBS media (**Fig. 2C** right panel). Increased growth rates of MM361 LTEDs in CSS media are suggestive of hormone-

independent growth and a more aggressive nature (LTEDs being more aggressive than parentals), consistent with the isolation of MM361 from brain metastatic BCa (39).

Next, we evaluated our HER2+/ER+ parental/LTED pair growth response to HER2- and ER-targeted therapies: dual HER2 blockade by TP, and fulvestrant (ICI) as a selective estrogen receptor degrader (SERD). For BT474, LTED growth was significantly inhibited by TP and minimally inhibited by ICI, whereas both TP and ICI caused significant growth inhibition of parental cells (**Fig. 2D**, left panel). Compared to parental MM361, both MM361 LTED variants were also less responsive to ICI but more responsive to TP. Additionally, results from western blot analysis showed no difference in ER protein levels of BT474 and MM361 LTEDs upon treatment with ICI versus vehicle, supporting the loss of ICI-mediated growth inhibition in HER2+/HR+ ETR LTEDs (**Fig. S1A** and **S1B**, (28)). Altogether, data shows that our two HER2+/ER+ LTED models differ from their parental counterparts in base line growth and responses to HER2- and ER-targeted therapies.

***MM361, but not BT474, LTEDs lose ER expression and E2-induced ER target gene expression***

We further characterized our HER2+/ER+ ETR models to determine if alterations in the basal expression of ER and HER family members may explain observed differential growth inhibition of parental/LTED pair models to anti-HER2 and ER treatments. When compared to their corresponding parentals, BT474 LTEDs showed no substantial changes in ER protein or *ESR1* transcript levels, whereas a significant reduction of both was observed in MM361 LTEDs (**Fig. 3A** to **3C**). Additionally, ER transcriptional activity was confirmed by increased expression of ER-target genes (*PGR* and *TFF1*) upon E2 stimulation only in LTEDs of BT474, but not MM361 (**Fig. 3D**). Protein analysis of the HER family revealed a significant upregulation of EGFR and a modest increase of HER3 in BT474 LTEDs (**Fig. 3A** and **3B**). A significant increase in HER2

and/or modest increase in EGFR (which is able to form heterodimers with HER2 (40)) protein levels of MM361 LTEDs (**Fig. 3A** and **3B**) may explain why these cells responded better to growth inhibition by TP than parentals (**Fig. 2D**). LTED variants of both BT474 and MM361 cell lines showed activation of the pro-survival AKT signaling (pAKT) downstream of HER2 (**Fig. 3A** and **3B**).

***MM361 LTEDs gain basal-like and HER2-enriched intrinsic subtypes and exonic mutations in genes encoding transcription factors and chromatin modifiers***

Resistance to ET may arise due to changes in gene transcription and/or mutational alterations. The loss/downregulation of ER and increase in HER2 expression in the MM361 LTED model (**Fig. 3**), coupled with their more rapid adaptation to LTED conditions and increased growth rate vs. parentals (**Fig. 2C**), raised the question of whether this model has shifted its intrinsic subtypes. Data from the SONABRE registry study supports this notion, reporting that HER2+/ER+ BCa has the highest rate of subtype discordance at metastatic presentation (41). We therefore prioritized the MM361 LTED model for further transcriptomic and genomic analyses to identify putative molecular mechanisms driving resistance. We first performed scRNAseq and analyzed the molecular subtype of individual cells using PAM50. MM361 LTEDs intrinsic subtyping is discordant from its parentals. As might be predicted from their loss/downregulation of ER expression at the mRNA and protein levels, LTEDs demonstrated a shift towards non-luminal HER2-enriched (HER2-E) and basal-like phenotypes (**Fig. 4A** and **4B**). Additionally, we performed whole-genome sequencing to identify mutations gained in MM361 LTED. Analysis of SBS mutational signatures from our WGS data showed an enrichment in C to T base substitutions (SBS1) as well as T to C base substitutions (SBS5) across the genome of MM361 LTEDs compared to the parental cell line (**Fig. 4C**). These aging-related, clock-like mutational signatures are prevalent in many cancer types, though SBS1 mutations were recently reported to be enriched in breast cancer metastases in an age-

independent manner (42). Next, we focused on mutated genes at their exonic regions. MM361 LTEDA and B shared a total of 70 genes bearing mutations in their exonic regions when compared to their parental cells (**Fig. 4D**). After excluding the 22 genes with silent mutations and characterizing the mutational signatures of the remaining 48, C to T and C to A were the most predominant mutation types (**Fig. 4E** and **Table S2** (28)). Most of these mutated genes were modestly deleterious (**Fig. 4F**) as predicted by Varmap (43). These genes mainly encode for transcription factors and chromatin modifiers, namely *HEY1*, *CHD4*, *MAFF*, *PRDM14*, *SATB2*, *SUPT6H*, *ZNF135*. Importantly, mutation of one or more of these genes is significantly enriched in ETR advanced breast cancers that are HER2+ and/or progesterone receptor-negative (PR-; **Fig. S2A** and **S2B** (28)). Together, these data show that a shift towards more aggressive intrinsic molecular subtypes (basal and HER2-enriched) and acquiring mutated transcription factors and chromatin modifiers accompanies the development of ETR in the MM361 LTED model.

***Lipid metabolism pathways are upregulated in the MM361 LTEDs***

Using our scRNAseq data, we performed unsupervised clustering using Seurat to identify over- and under-represented cell populations in MM361 parental and LTED A and B cells (**Fig. S3** (28)). We identified seven clusters, with clusters 2 and 5 enriched in parental cells and clusters 0 and 6 enriched in LTED cells (**Fig. S3A** to **S3C** (28)). GSEA analysis showed that parental-dominant clusters 2 and 5 were enriched with genes regulating estrogen response, glycolysis, TCA cycle, and oxidative phosphorylation (**Fig. S3D** (28)). By contrast, LTED-dominant clusters showed a significant overrepresentation of fatty acid metabolism (in the more abundant cluster 0), and RNA processing pathways e.g., nonsense-mediated decay (in the less abundant cluster 6). We then constructed “pseudo-bulk” profiles from scRNAseq and performed differential expression analysis of transcriptomic changes that characterize MM361 LTEDA and B vs. parental cells. Transcriptional profiling at a false discovery rate (FDR) <0.05 and a log2 fold

358 change ≤-0.5 and ≥0.5 identified a total of 356 differentially expressed genes (DEG) between
359 parental and LTEDA, and 674 DEG between parental and LTEDB (**Fig. 5A**). The intersection of
360 DEG from LTED vs. parental comparisons resulted in 202 DEG between both LTED lines and
361 parental cells, with 156 and 46 genes being upregulated and downregulated, respectively (**Fig.**
362 **5B** and **Table S3** (28)). We validated the transcriptomic analysis of MM361 LTEDs and
363 confirmed the increased expression of eleven upregulated DEGs using qRT-PCR (**Fig. 5C**).
364 Importantly, *ESR1* and *TFF1* were among the top downregulated genes and *ERBB2* expression
365 was upregulated (**Fig. S4** (28)), consistent with data shown in **Fig. 3**. Using LISA (44) to predict
366 the transcriptional regulators (TRs) of these DEGs (**Table S3** (28)), we found that the steroid
367 hormone receptors *PGR*, *ESR1*, and *AR*, as well as the pioneer factors *GRHL2* and *FOXA1*
368 were among the most enriched TRs in common for both up- and downregulated DEGs.
369 Predicted TRs associated exclusively with downregulated DEGs included *E2F1*, *RARA*, and
370 *MAFB* (a homolog of *MAFF*, which we identified as mutated in LTED cells, **Table S2** (28)).
371 Predicted TRs for upregulated DEGs included *GATA2*, *PPARG*, and *CEBPA*.
372
373 To identify biological processes that are enriched within the LTED variants, we performed GSEA
374 on the upregulated and downregulated shared gene lists of both LTED lines vs. parental cells.
375 Genes upregulated in LTEDs were enriched in pathways involved in defective apoptosis and
376 immune-related pathways. Conversely, pathways involved in estrogen and other nuclear
377 receptor signaling were enriched within the downregulated gene set (**Fig. 5D**). Notably,
378 metabolic pathways were among the enriched pathways in the MM361 LTEDs. While lipid
379 metabolism was upregulated, pathways of glucose metabolism, glycolysis and gluconeogenesis
380 were all downregulated (**Fig. 5D**), consistent with our unsupervised clustering analysis results
381 (**Fig. S3** (28)). The upregulation of lipid metabolism pathways is also supported by the observed
382 enrichment of putative TRs *PPARG* and *CEBPA* from our upregulated DEGs (**Table S3** (28)),

383 which are key activators of lipid metabolism (45). Our data suggest notable metabolic
384 remodeling of MM361 LTEDs, specifically upregulation of lipid metabolism.
385
386 ***Dual targeting of HER2 and GPX4 increase cell death of HER2+/ER+ LTEDs***
387 *ALOX15B* and *GPX4* are two of the upregulated genes of lipid metabolism pathways enriched in
388 the MM361 LTEDs (**Fig. 5D** and **5E**). In addition, *ALOX15B* and *GPX4* were among the 13
389 MM361 LTED DEGs that overlapped with ferroptosis-related genes (**Fig. S5** (28)). Ferroptosis is
390 an iron-dependent cell death that is triggered by lipid peroxidation (46). Interestingly, both
391 upregulated proteins are opposing key players in regulating ferroptosis (47); ALOX15B induces
392 ferroptosis, whereas GPX4 inhibits it. We validated the upregulation of *ALOX15B* mRNA in
393 MM361 LTEDs (**Fig. 5C**), and GPX4 protein levels in both MM361 and BT474 LTEDs (**Fig. 6A**
394 and **S6A** (28)).
395
396 Inhibiting the PI3K-AKT-mTOR signaling pathway – which we show in **Fig. 3** is strongly
397 activated in both MM361 and BT474 LTED cells – can sensitize BCa cells to ferroptosis
398 induction, in part by reducing SREBP-mediated lipogenesis (48). Therefore, we hypothesized
399 that LTED cells of HER2+/ER+ BCa are resistant to ferroptosis, due to GPX4 upregulation, and
400 that dual targeting of HER2 (upstream of PI3K-AKT-mTOR) and GPX4 may sensitize these
401 LTEDs to ferroptosis-induced cell death. In MM361 LTEDs, significant cell death was observed
402 following HER2 inhibition by TP, but not GPX4 inhibition by RSL3 (**Fig. 6B** and **6C**). In BT474
403 LTEDs, TP and RSL3 alone each significantly increased cell death (**Fig. S6B** and **S6C** (28)).
404 Importantly, in both LTED models, cell death was significantly enhanced by the combination of
405 TP + RSL3. As expected, TP alone reduced the activation of AKT (pAKT) and RSL3 alone
406 reduced protein levels of GPX4 (**Fig. 6D)**, but no further reduction was observed with TP +
407 RSL3 vs. that of the single treatments (**Fig. 6D**). To test whether the increased cell death
408 induced by the TP + RSL3 combination was due to ferroptosis, we measured the levels of two

ferroptosis lipid peroxidation markers, 4-hydroxynonenal (4-HNE) and malondialdehyde (MDA) (**Fig. S7** (28)). RSL3 alone slightly increased levels of both 4-HNE and MDA, but TP + RSL3 did not further enhance the levels of 4-HNE and MDA protein conjugates. Together, these data suggest that increased lipid metabolism in HER2+/ER+ BCa LTED models is accompanied by reprogramming of ferroptosis pathways, and that the combination of anti-HER2 agents and a ferroptosis inducer is an effective approach to inducing cell death.

## DISCUSSION

To date, models of acquired ETR have been almost exclusively developed for HER2-/ER+ BCa, and not HER2+/ER+. In this study, we generated and characterized models of the latter without using genetic manipulation approaches. We report that ETR BT474 and MM361 AI-resistant (LTED) models capture distinct phenotypes of HER2+/ER+ BCa as supported by the following results. Compared to parentals, MM361 LTEDs grew faster, lost ER, and increased HER2 expression, whereas BT474 LTEDs grew slower and showed no substantial changes in ER or HER2 expression. Additionally, growth inhibition by anti-HER2 (TP) treatment was much more pronounced in the LTEDs vs. parental MM361, unlike the BT474 model, where both LTEDs and parentals benefited from TP. Differences in ER and HER2 expression in the LTEDs of MM361 and BT474 models may suggest distinct resistance mechanisms to ET partly due to the differential distribution of intrinsic subtypes within these two cell lines. It could imply that BT474 ETR behaves more like luminal whereas MM361 LTEDs behaves more like non-luminal HER2+ BCa and hence the more aggressive nature of the latter.

HR and HER2 receptor expressions, or lack thereof, are critical in guiding BCa treatments. However, pathology-based immunohistochemistry (IHC) does not fully recapitulate intrinsic biology. Instead, substantial discrepancies exist between IHC-based and gene expression-based PAM50 subtyping (49). Our results show that MM361 LTEDs intrinsic subtyping is

435 discordant from its parentals. We observed a loss in ER/*ESR1* accompanied by a gain in
436 HER2/*ERBB2* expression and, thus, molecular switching to non-luminal HER2-E phenotype and
437 sustained activation of AKT signaling. These alterations altogether explain why our ETR MM361
438 LTEDs were less responsive to ICI but more responsive to anti-HER2 targeted therapies vs.
439 their corresponding TP-resistant parentals. HER2-E subtype represents ~75% HER2+/HR- and
440 30% of HER2+/HR+ tumors (49,50), is associated with anti-HER2 sensitivity (49), and is a
441 predictive biomarker of poor response and resistance to AI (10). Our findings are supported by
442 several studies. First, data from the SONABRE registry (NCT03577197) show that among all
443 BCa subtypes, patients with HR+/HER2+ advanced BC exhibit the highest receptor subtype
444 discordance rate between primary tumor and metastatic lesions as they convert mainly to
445 HR+/HER2- and HR-/HER2+ (41). In other words, ER and HER2 expressions varied during
446 tumor progression, and cross-talk between ER and HER2 was proposed as the leading cause of
447 this discordance (41). Second, HER2 and ER expressions are negatively correlated in HER2+
448 BCa tumors (51). Third, cell lineage tracing experiments in mice showed that HER2+/ER+ cells
449 can lose ER expression and be converted into highly aggressive HER2+/ER- BCa cells (52).
450 Lastly, HER2 overexpression (with or without EGFR) activates downstream AKT and MAPK
451 pathways to circumvent ER inhibition and promotes growth of ETR BCa (2,25,53). ER loss in our
452 MM361 ETR model could be explained by *ESR1* promoter methylation and/or decreased FOXA1
453 and GATA3, which are required for normal ER expression (52). Additionally, losing the ER-
454 regulated cluster of let-7c, miR99a, and miR125b (54), could explain our upregulated HER2
455 expression.
456
457 Beyond the HER2-E intrinsic subtype, acquiring mutations in genes encoding for transcription
458 factors and chromatin modifiers could underlie mechanisms of AI resistance and/or the
459 aggressive nature of the MM361 LTED model. For example, integrated genomic analysis of
460 responding vs. resistant ER+ breast tumors from a patient who developed resistance to

461 letrozole treatment revealed an acquired mutation in the *CHD4* gene (55). SUPT6H protein
462 levels decrease in poorly differentiated breast tumors, and SUPT6H is a requirement for ERα
463 transcriptional activity and maintenance of chromatin structure in BCa cells (56). Also, SATB2
464 induces transformation of mammary epithelial cells into progenitor-like cells and its knockdown
465 attenuates proliferation and epithelial-mesenchymal transition (EMT) of BCa cells (57). What
466 role the mutations in these genes that we observe in MM361 LTEDs play in the ETR phenotype
467 is a subject of future study.
468
469 BCa cells carrying *PIK3CA* activating mutation (like the parental BT474 and MM361 cells (58)),
470 and thus an activated PI3K-AKT-mTOR signaling pathway, are resistant to ferroptosis induction
471 by the GPX4 inhibitor RSL3 (48). Consistent with this, inhibiting an activated PI3K-AKT-mTOR
472 signaling pathway sensitizes BCa cells to ferroptosis induction by RSL3 (48). In the current
473 study, we show that dual targeting of HER2 and GPX4 increases cell death of HER2+/ER+
474 LTEDs but not levels of ferroptosis lipid peroxidation markers beyond that of single-agent
475 treatments. One possible explanation could be that GPX4 inhibition may not be sufficient to
476 overcome ferroptosis resistance in our LTEDs. In other words, elevated GPX4 may not be the
477 sole cause of ferroptosis resistance in MM361 LTEDs; instead, several other ferroptosis-related
478 DEGs may mediate this resistance. Dysregulated oxidative and iron homeostasis exemplified by
479 upregulation of ferroptosis suppressor genes (*TMBIM4* and *GPX4*), antioxidants (*PRDX2*), iron
480 chelators (*LCN2*), and/or downregulation of ferroptosis inducing genes (*RPL8* and *HILPDA*)
481 could be responsible for ferroptosis resistance in our LTEDs (**Fig. S3** (28)). Moreover, multiple
482 ferroptosis regulatory pathways that are independent of GPX4 have recently been discovered
483 (59). For example, cisplatin-resistant-derived exosomes secrete microRNAs that increase the
484 expression of ferroptosis suppressor protein 1 (FSP1) and thus enhance resistance of cancer
485 cells to ferroptosis (60). Along the same lines, LTED cells treated with TP + RSL3 may protect
486 themselves from ferroptosis using a similar mechanism. In our hands, TP did not reduce GPX4

nor enhance expression of ferroptosis lipid peroxidation markers. However, a recent study reported that trastuzumab triggers ferroptosis by reducing GPX4 whilst increasing ROS levels in embryonic rat myoblast (H9c2) cells (61). This inconsistency could be attributed to variances in cell context, doses and/or duration of treatments.

Inevitably, our study has several limitations that must be considered. Future xenograft studies will be necessary to verify and follow up on some of our current findings, for example, the response of ETR HER2+/ER+ to ET and anti-HER2 treatments and whether ferroptosis induction combined with anti-HER2 treatments suppresses the growth of these cells *in vivo*. Despite harboring a sufficient gain in *ERBB2* copy number to be classified as HER2+ (amplified, (62,63)), a previous study demonstrated that the parental MM361 cell line exhibits heterogenous expression of *ERBB2* and *ESR1*, and this heterogeneity is not due to heritable genetic differences (63), suggesting a high degree of plasticity and variability. This informed our rationale for performing scRNAseq to capture transcriptional heterogeneity of the parental cells and ETR LTED models. Importantly, our conventional and “pseudo-bulk” analyses of the scRNAseq data both identified alterations in lipid metabolism. However, we sequenced a relatively small number of cells by scRNAseq (<4000 cells per sample), and combined with the fact that scRNAseq is best suited to detecting higher abundance transcripts, we cannot exclude the possibility that we are missing minor populations or subclones that contribute significantly to the ETR phenotype (e.g. (64,65)). The gene mutations we identified in LTEDs are constrained by the WGS coverage that we achieved (LTEDA: 53x, LTEDB: 50x, Parental: 52x). Furthermore, deeper sequencing depths may capture and result in a larger number of mutated genes. However, even at the sequencing depths and coverage levels we used, our results may suggest that multiple potential resistance mechanisms exist. Deep sequencing of a different epithelial tumor, colorectal cancer, coupled with an evolutionary analysis, showed that the ~$10^9$ cells in a 1 $cm^3$ lesion will contain every possible resistance mutation in a minor subclone within the lesion (66).

513 This large diversity of resistance mechanisms implies a need for treatment regimens that
514 include therapies too numerous to be given simultaneously in combination (67).
515
516 Increasing efforts are being directed toward chemotherapy-sparing regimens for HER2+/ER+
517 BCa (68-71). However, these treatment strategies should also be tested on HER2+/ER+ BCa
518 that are refractory to or have progressed on ET. Therefore, future studies are needed to
519 address open questions regarding 1) responsiveness of ETR HER2+/ER+ models to dual and
520 triple combinations of anti-HER2, ET/SERDs (including recently approved oral SERD
521 amcenestrant), and CDK4/6 inhibitors, as well as innovative sequencing of these combinations
522 (63,64,67,72), 2) the impact of our identified mutations on development of ETR in HER2+/ER+
523 BCa, and 3) differences in ER activity between ETR models of HER2+/ER+ (as BT474) and
524 other HER2-ER+.
525
526 **CONCLUSIONS**
527 Characterizing models of HER2+/ER+ that mimic a real-world treatment pattern is necessary to
528 understand mechanisms of resistance to ET and may provide useful information for refining
529 current treatment approaches and improving patients' outcomes. Here, we report that anti-
530 HER2 targeted therapies effectively inhibit growth of ETR HER2+/ER+ BCa cells that exhibit
531 concurrent loss of ER expression and gain in HER2 and HER2-E phenotype. Our BT474 and
532 MM361 AI-resistant models capture distinct phenotypes of HER2+/ER+ BCa and pinpoint
533 altered lipid metabolism and ferroptosis remodeling as vulnerabilities of this type of ETR BCa.
534
535 **ABBREVIATIONS**
536 4-HNE: 4-hydroxynonenal; BCa: Breast cancer; BT474: BT-474; CSS: Charcoal-stripped bovine
537 serum; DEG: Differential expressed gene; DMFS: Distant metastasis-free survival; E2: 17β-
538 estradiol; EMT: epithelial-mesenchymal transition; ER: Estrogen receptor; ET: Endocrine

539 therapy; ETR: Endocrine therapy-resistant; FDR: False discovery rate; FSP1: Ferroptosis
540 suppressor protein 1; GSEA: Gene set enrichment assay; HER2: human epidermal growth
541 factor receptor 2; HR: Hormone receptor; ICI: fulvestrant; IMEM: Improved minimum essential
542 medium; LTED: Long-term estrogen deprivation; MDA: Malondialdehyde; MM361: MDA-MB-
543 361; MSigDB: Molecular signature database; OS: Overall survival; PFS: Progression-free
544 survival; qRT-PCR: Real-time PCR; RFS: Relapse-free survival; SBS: Single base substitution;
545 scRNAseq: Single-cell RNA sequencing; SERD: Selective estrogen receptor degrader; TR:
546 Transcriptional regulator; TP: Trastuzumab + pertuzumab; WGS: whole genome sequencing
547

548 **DECLARATIONS**

549 ***Acknowledgements***

550 The authors would like to thank members of the Riggins laboratory, Drs. Michael Johnson, Marc
551 Lippman, and Joyce Slingerland (Lombardi Comprehensive Cancer Center, Georgetown
552 University), and members of NR IMPACT for sharing reagents, scientific insights, and/or
553 technical assistance.
554

555 ***Data Availability***

556 Original data generated and analyzed during this study are included in this published article or
557 in the data repository listed in References ((28); https://doi.org/10.5281/zenodo.8265999).
558

559 ***Authors' contributions***

560 SB, HS and RBR designed the experiments. SB performed most of the experiments, analyzed
561 data, prepared figures, and drafted the manuscript. HS performed, analyzed, and graphed some
562 of the RT-PCR and growth assays. MB and MP performed the scRNAseq experiments and LJ
563 analyzed the scRNAseq and WGS data. ST and DM handled most of the western blot analyses.
564 MDM and RAB contributed to the study discussions. RBR supervised the study, wrote parts of

565 the manuscript, reviewed, and revised it. All authors read, revised, and approved the final
566 manuscript.
567
568 ***Ethics approval and consent to participate***
569 Not applicable.
570
571 ***Consent for publication***
572 All authors agreed to publish this study.
573

## REFERENCES


1. Sung H, Ferlay J, Siegel RL, Laversanne M, Soerjomataram I, Jemal A, Bray F. Global Cancer Statistics 2020: GLOBOCAN Estimates of Incidence and Mortality Worldwide for 36 Cancers in 185 Countries. *CA Cancer J Clin*. 2021;71(3):209-249.
2. Alataki A, Dowsett M. Human epidermal growth factor receptor-2 and endocrine resistance in hormone-dependent breast cancer. *Endocr Relat Cancer*. 2022;29(8):R105-R122.
3. Azim HA, Jr., Piccart MJ. Simultaneous targeting of estrogen receptor and HER2 in breast cancer. *Expert Rev Anticancer Ther*. 2010;10(8):1255-1263.
4. Vaz-Luis I, Winer EP, Lin NU. Human epidermal growth factor receptor-2-positive breast cancer: does estrogen receptor status define two distinct subtypes? *Ann Oncol*. 2013;24(2):283-291.
5. Park YH, Lee S, Cho EY, Choi YL, Lee JE, Nam SJ, Yang JH, Ahn JS, Im YH. Patterns of relapse and metastatic spread in HER2-overexpressing breast cancer according to estrogen receptor status. *Cancer Chemother Pharmacol*. 2010;66(3):507-516.
6. Vaz-Luis I, Ottesen RA, Hughes ME, Marcom PK, Moy B, Rugo HS, Theriault RL, Wilson J, Niland JC, Weeks JC, Lin NU. Impact of hormone receptor status on patterns of recurrence and clinical outcomes among patients with human epidermal growth factor-2-positive breast cancer in the National Comprehensive Cancer Network: a prospective cohort study. *Breast Cancer Res*. 2012;14(5):1-14.
7. Arciero CA, Guo Y, Jiang R, Behera M, O'Regan R, Peng L, Li X. ER+/HER2+ Breast Cancer Has Different Metastatic Patterns and Better Survival Than ER-/HER2+ Breast Cancer. *Clin Breast Cancer*. 2019;19(4):236-245.
8. Han Y, Wu Y, Xu H, Wang J, Xu B. The impact of hormone receptor on the clinical outcomes of HER2-positive breast cancer: a population-based study. *Int J Clin Oncol*. 2022;27(4):707-716.
9. Martinez-Saez O, Prat A. Current and Future Management of HER2-Positive Metastatic Breast Cancer. *JCO Oncol Pract*. 2021;17(10):594-604.
10. Bergamino MA, López-Knowles E, Morani G, Tovey H, Kilburn L, Schuster EF, Alataki A, Hills M, Xiao H, Holcombe C, Skene A, Robertson JF, Smith IE, Bliss JM, Dowsett M, Cheang MCU. HER2-enriched subtype and novel molecular subgroups drive aromatase inhibitor resistance and an increased risk of relapse in early ER+/HER2+ breast cancer. *EBioMedicine*. 2022;83:104205.
11. Ellis MJ, Tao Y, Young O, White S, Proia AD, Murray J, Renshaw L, Faratian D, Thomas J, Dowsett M, Krause A, Evans DB, Miller WR, Dixon JM. Estrogen-Independent Proliferation Is Present in Estrogen-Receptor HER2-Positive Primary Breast Cancer After Neoadjuvant Letrozole. *Journal of Clinical Oncology*. 2006;24(19):3019-3025.
12. Kaufman B, Mackey JR, Clemens MR, Bapsy PP, Vaid A, Wardley A, Tjulandin S, Jahn M, Lehle M, Feyereislova A, Révil C, Jones A. Trastuzumab plus anastrozole versus anastrozole alone for the treatment of postmenopausal women with human epidermal growth factor receptor 2-positive, hormone receptor-positive metastatic breast cancer: results from the randomized phase III TAnDEM study. *J Clin Oncol*. 2009;27(33):5529-5537.
13. Huober J, Fasching PA, Barsoum M, Petruzelka L, Wallwiener D, Thomssen C, Reimer T, Paepke S, Azim HA, Ragosch V, Kubista E, Baumgärtner AK, Beckmann MW, May C, Nimmrich I, Harbeck N. Higher efficacy of letrozole in combination with trastuzumab compared to letrozole monotherapy as first-line treatment in patients with HER2-positive, hormone-receptor-positive metastatic breast cancer - results of the eLEcTRA trial. *Breast*. 2012;21(1):27-33.

14. Rimawi M, Ferrero JM, de la Haba-Rodriguez J, Poole C, De Placido S, Osborne CK, Hegg R, Easton V, Wohlfarth C, Arpino G. First-Line Trastuzumab Plus an Aromatase Inhibitor, With or Without Pertuzumab, in Human Epidermal Growth Factor Receptor 2-Positive and Hormone Receptor-Positive Metastatic or Locally Advanced Breast Cancer (PERTAIN): A Randomized, Open-Label Phase II Trial. *J Clin Oncol*. 2018;36(28):2826-2835.
15. Statler AB, Hobbs BP, Wei W, Gupta A, Blake CN, Nahleh ZA. Real-world Treatment Patterns and Outcomes in HR+/HER2+ Metastatic Breast Cancer Patients: A National Cancer Database Analysis. *Sci Rep*. 2019;9(1):1-10.
16. Ibragimova KIE, Geurts SME, Meegdes M, Erdkamp F, Heijns JB, Tol J, Vriens B, Dercksen MW, Aaldering KNA, Pepels M, van de Winkel L, Peters N, Teeuwen-Dedroog NJA, Vriens IJH, Tjan-Heijnen VCG. Outcomes for the first four lines of therapy in patients with HER2-positive advanced breast cancer: results from the SONABRE registry. *Breast Cancer Res Treat*. 2023:1-13.
17. Cardoso F, Paluch-Shimon S, Senkus E, Curigliano G, Aapro MS, Andre F, Barrios CH, Bergh J, Bhattacharyya GS, Biganzoli L, Boyle F, Cardoso MJ, Carey LA, Cortes J, El Saghir NS, Elzayat M, Eniu A, Fallowfield L, Francis PA, Gelmon K, Gligorov J, Haidinger R, Harbeck N, Hu X, Kaufman B, Kaur R, Kiely BE, Kim SB, Lin NU, Mertz SA, Neciosup S, Offersen BV, Ohno S, Pagani O, Prat A, Penault-Llorca F, Rugo HS, Sledge GW, Thomssen C, Vorobiof DA, Wiseman T, Xu B, Norton L, Costa A, Winer EP. 5th ESO-ESMO international consensus guidelines for advanced breast cancer (ABC 5). *Ann Oncol*. 2020;31(12):1623-1649.
18. Giordano SH, Franzoi MAB, Temin S, Anders CK, Chandarlapaty S, Crews JR, Kirshner JJ, Krop IE, Lin NU, Morikawa A, Patt DA, Perlmutter J, Ramakrishna N, Davidson NE. Systemic Therapy for Advanced Human Epidermal Growth Factor Receptor 2-Positive Breast Cancer: ASCO Guideline Update. *J Clin Oncol*. 2022;40(23):2612-2635.
19. Dowsett M, Allred C, Knox J, Quinn E, Salter J, Wale C, Cuzick J, Houghton J, Williams N, Mallon E, Bishop H, Ellis I, Larsimont D, Sasano H, Carder P, Cussac AL, Knox F, Speirs V, Forbes J, Buzdar A. Relationship between quantitative estrogen and progesterone receptor expression and human epidermal growth factor receptor 2 (HER-2) status with recurrence in the Arimidex, Tamoxifen, Alone or in Combination trial. *J Clin Oncol*. 2008;26(7):1059-1065.
20. Cortes J, Baselga J. How to treat hormone receptor-positive, human epidermal growth factor receptor 2-amplified breast cancer. *J Clin Oncol*. 2009;27(33):5492-5494.
21. Schiff R, Massarweh SA, Shou J, Bharwani L, Mohsin SK, Osborne CK. Cross-talk between estrogen receptor and growth factor pathways as a molecular target for overcoming endocrine resistance. *Clin Cancer Res*. 2004;10(1 Pt 2):331s-336s.
22. Dowsett M, Ebbs SR, Dixon JM, Skene A, Griffith C, Boeddinghaus I, Salter J, Detre S, Hills M, Ashley S, Francis S, Walsh G, Smith IE. Biomarker changes during neoadjuvant anastrozole, tamoxifen, or the combination: influence of hormonal status and HER-2 in breast cancer--a study from the IMPACT trialists. *J Clin Oncol*. 2005;23(11):2477-2492.
23. Bender LM, Nahta R. Her2 cross talk and therapeutic resistance in breast cancer. *Front Biosci*. 2008;13:3906-3912.
24. Chung YL, Sheu ML, Yang SC, Lin CH, Yen SH. Resistance to tamoxifen-induced apoptosis is associated with direct interaction between Her2/neu and cell membrane estrogen receptor in breast cancer. *Int J Cancer*. 2002;97(3):306-312.
25. Shou J, Massarweh S, Osborne CK, Wakeling AE, Ali S, Weiss H, Schiff R. Mechanisms of tamoxifen resistance: increased estrogen receptor-HER2/neu cross-talk in ER/HER2-positive breast cancer. *J Natl Cancer Inst*. 2004;96(12):926-935.
26. Neve RM, Chin K, Fridlyand J, Yeh J, Baehner FL, Fevr T, Clark L, Bayani N, Coppe JP, Tong F, Speed T, Spellman PT, DeVries S, Lapuk A, Wang NJ, Kuo WL, Stilwell JL,

Pinkel D, Albertson DG, Waldman FM, McCormick F, Dickson RB, Johnson MD, Lippman M, Ethier S, Gazdar A, Gray JW. A collection of breast cancer cell lines for the study of functionally distinct cancer subtypes. *Cancer Cell*. 2006;10(6):515-527.

27. Dai X, Cheng H, Bai Z, Li J. Breast Cancer Cell Line Classification and Its Relevance with Breast Tumor Subtyping. *J Cancer*. 2017;8(16):3131-3141.

28. Bahnassy S, Stires H, Jin L, Tam S, Mobin D, Balachandran M, Podar M, McCoy MD, Beckman RA, Riggins RB. Data from: Data from: Unraveling vulnerabilities in endocrine therapy-resistant HER2+/ER+ breast cancer 2023. Deposited Deposited 19 August 2023. https://zenodo.org/record/8266000.

29. Macosko EZ, Basu A, Satija R, Nemesh J, Shekhar K, Goldman M, Tirosh I, Bialas AR, Kamitaki N, Martersteck EM, Trombetta JJ, Weitz DA, Sanes JR, Shalek AK, Regev A, McCarroll SA. Highly Parallel Genome-wide Expression Profiling of Individual Cells Using Nanoliter Droplets. *Cell*. 2015;161(5):1202-1214.

30. Hao Y, Hao S, Andersen-Nissen E, Mauck WM, 3rd, Zheng S, Butler A, Lee MJ, Wilk AJ, Darby C, Zager M, Hoffman P, Stoeckius M, Papalexi E, Mimitou EP, Jain J, Srivastava A, Stuart T, Fleming LM, Yeung B, Rogers AJ, McElrath JM, Blish CA, Gottardo R, Smibert P, Satija R. Integrated analysis of multimodal single-cell data. *Cell*. 2021;184(13):3573-3587 e3529.

31. Gendoo DM, Ratanasirigulchai N, Schroder MS, Pare L, Parker JS, Prat A, Haibe-Kains B. Genefu: an R/Bioconductor package for computation of gene expression-based signatures in breast cancer. *Bioinformatics*. 2016;32(7):1097-1099.

32. Subramanian A, Tamayo P, Mootha VK, Mukherjee S, Ebert BL, Gillette MA, Paulovich A, Pomeroy SL, Golub TR, Lander ES, Mesirov JP. Gene set enrichment analysis: a knowledge-based approach for interpreting genome-wide expression profiles. *Proc Natl Acad Sci U S A*. 2005;102(43):15545-15550.

33. Andrews S. FastQC: a quality control tool for high throughput sequence data. Babraham Bioinformatics, Babraham Institute, Cambridge, United Kingdom; 2010.

34. Martin M. Cutadapt removes adapter sequences from high-throughput sequencing reads. *2011*. 2011;17(1):3.

35. Li H, Durbin R. Fast and accurate short read alignment with Burrows-Wheeler transform. *Bioinformatics*. 2009;25(14):1754-1760.

36. Van der Auwera GA, O'Connor BD. Genomics in the cloud: using Docker, GATK, and WDL in Terra. O'Reilly Media.

37. Alexandrov LB, Kim J, Haradhvala NJ, Huang MN, Tian Ng AW, Wu Y, Boot A, Covington KR, Gordenin DA, Bergstrom EN, Islam SMA, Lopez-Bigas N, Klimczak LJ, McPherson JR, Morganella S, Sabarinathan R, Wheeler DA, Mustonen V, Group PMSW, Getz G, Rozen SG, Stratton MR, Consortium P. The repertoire of mutational signatures in human cancer. *Nature*. 2020;578(7793):94-101.

38. Gyorffy B, Lanczky A, Eklund AC, Denkert C, Budczies J, Li Q, Szallasi Z. An online survival analysis tool to rapidly assess the effect of 22,277 genes on breast cancer prognosis using microarray data of 1,809 patients. *Breast Cancer Res Treat*. 2010;123(3):725-731.

39. Cailleau R, Olive M, Cruciger QV. Long-term human breast carcinoma cell lines of metastatic origin: preliminary characterization. *In Vitro*. 1978;14(11):911-915.

40. Bai X, Sun P, Wang X, Long C, Liao S, Dang S, Zhuang S, Du Y, Zhang X, Li N, He K, Zhang Z. Structure and dynamics of the EGFR/HER2 heterodimer. *Cell Discov*. 2023;9(1):18.

41. Meegdes M, Ibragimova KIE, Lobbezoo DJA, Vriens IJH, Kooreman LFS, Erdkamp FLG, Dercksen MW, Vriens B, Aaldering KNA, Pepels M, van de Winkel LMH, Tol J, Heijns JB, van de Wouw AJ, Peters N, Hochstenbach-Waelen A, Smidt ML, Geurts SME, Tjan-Heijnen VCG. The initial hormone receptor/HER2 subtype is the main determinator of

subtype discordance in advanced breast cancer: a study of the SONABRE registry. *Breast Cancer Res Treat*. 2022;192(2):331-342.

42. Martinez-Jimenez F, Movasati A, Brunner SR, Nguyen L, Priestley P, Cuppen E, Van Hoeck A. Pan-cancer whole-genome comparison of primary and metastatic solid tumours. *Nature*. 2023;618(7964):333-341.
43. Stephenson JD, Laskowski RA, Nightingale A, Hurles ME, Thornton JM. VarMap: a web tool for mapping genomic coordinates to protein sequence and structure and retrieving protein structural annotations. *Bioinformatics*. 2019;35(22):4854-4856.
44. Qin Q, Fan J, Zheng R, Wan C, Mei S, Wu Q, Sun H, Brown M, Zhang J, Meyer CA, Liu XS. Lisa: inferring transcriptional regulators through integrative modeling of public chromatin accessibility and ChIP-seq data. *Genome Biol*. 2020;21(1):32.
45. Lefterova MI, Zhang Y, Steger DJ, Schupp M, Schug J, Cristancho A, Feng D, Zhuo D, Stoeckert CJ, Jr., Liu XS, Lazar MA. PPARgamma and C/EBP factors orchestrate adipocyte biology via adjacent binding on a genome-wide scale. *Genes Dev*. 2008;22(21):2941-2952.
46. Yan HF, Zou T, Tuo QZ, Xu S, Li H, Belaidi AA, Lei P. Ferroptosis: mechanisms and links with diseases. *Signal Transduct Target Ther*. 2021;6(1):49.
47. Cai Y, Yang Z. Ferroptosis and Its Role in Epilepsy. *Front Cell Neurosci*. 2021;15:696889.
48. Yi J, Zhu J, Wu J, Thompson CB, Jiang X. Oncogenic activation of PI3K-AKT-mTOR signaling suppresses ferroptosis via SREBP-mediated lipogenesis. *Proc Natl Acad Sci U S A*. 2020;117(49):31189-31197.
49. Cejalvo JM, Pascual T, Fernández-Martínez A, Brasó-Maristany F, Gomis RR, Perou CM, Muñoz M, Prat A. Clinical implications of the non-luminal intrinsic subtypes in hormone receptor-positive breast cancer. *Cancer Treat Rev*. 2018;67:63-70.
50. Prat A, Carey LA, Adamo B, Vidal M, Tabernero J, Cortés J, Parker JS, Perou CM, Baselga J. Molecular features and survival outcomes of the intrinsic subtypes within HER2-positive breast cancer. *J Natl Cancer Inst*. 2014;106(8):1-8.
51. Pinhel I, Hills M, Drury S, Salter J, Sumo G, A'Hern R, Bliss JM, Sestak I, Cuzick J, Barrett-Lee P, Harris A, Dowsett M, Group NABCTM. ER and HER2 expression are positively correlated in HER2 non-overexpressing breast cancer. *Breast Cancer Res*. 2012;14(2):1-12.
52. Ding Y, Liu Y, Lee DK, Tong Z, Yu X, Li Y, Xu Y, Lanz RB, O'Malley BW, Xu J. Cell lineage tracing links ERα loss in Erbb2-positive breast cancers to the arising of a highly aggressive breast cancer subtype. *Proc Natl Acad Sci U S A*. 2021;118(21):e2100673118.
53. Knowlden JM, Hutcheson IR, Jones HE, Madden T, Gee JM, Harper ME, Barrow D, Wakeling AE, Nicholson RI. Elevated levels of epidermal growth factor receptor/c-erbB2 heterodimers mediate an autocrine growth regulatory pathway in tamoxifen-resistant MCF-7 cells. *Endocrinology*. 2003;144(3):1032-1044.
54. Bailey ST, Westerling T, Brown M. Loss of Estrogen-Regulated microRNA Expression Increases HER2 Signaling and Is Prognostic of Poor Outcome in Luminal Breast Cancer. *Cancer Research*. 2015;75(2):436-445.
55. Xia Y, He X, Renshaw L, Martinez-Perez C, Kay C, Gray M, Meehan J, Parker JS, Perou CM, Carey LA, Dixon JM, Turnbull A. Integrated DNA and RNA Sequencing Reveals Drivers of Endocrine Resistance in Estrogen Receptor-Positive Breast Cancer. *Clin Cancer Res*. 2022;28(16):3618-3629.
56. Bedi U, Scheel AH, Hennion M, Begus-Nahrmann Y, Ruschoff J, Johnsen SA. SUPT6H controls estrogen receptor activity and cellular differentiation by multiple epigenomic mechanisms. *Oncogene*. 2015;34(4):465-473.

57. Yu W, Ma Y, Ochoa AC, Shankar S, Srivastava RK. Cellular transformation of human mammary epithelial cells by SATB2. *Stem Cell Res*. 2017;19:139-147.
58. Kataoka Y, Mukohara T, Shimada H, Saijo N, Hirai M, Minami H. Association between gain-of-function mutations in PIK3CA and resistance to HER2-targeted agents in HER2-amplified breast cancer cell lines. *Ann Oncol*. 2010;21(2):255-262.
59. Ma T, Du J, Zhang Y, Wang Y, Wang B, Zhang T. GPX4-independent ferroptosis-a new strategy in disease's therapy. *Cell Death Discov*. 2022;8(1):434.
60. Song Z, Jia G, Ma P, Cang S. Exosomal miR-4443 promotes cisplatin resistance in non-small cell lung carcinoma by regulating FSP1 m6A modification-mediated ferroptosis. *Life Sci*. 2021;276:119399.
61. Sun L, Wang H, Yu S, Zhang L, Jiang J, Zhou Q. Herceptin induces ferroptosis and mitochondrial dysfunction in H9c2 cells. *Int J Mol Med*. 2022;49(2):1-8.
62. Ghandi M, Huang FW, Jane-Valbuena J, Kryukov GV, Lo CC, McDonald ER, 3rd, Barretina J, Gelfand ET, Bielski CM, Li H, Hu K, Andreev-Drakhlin AY, Kim J, Hess JM, Haas BJ, Aguet F, Weir BA, Rothberg MV, Paolella BR, Lawrence MS, Akbani R, Lu Y, Tiv HL, Gokhale PC, de Weck A, Mansour AA, Oh C, Shih J, Hadi K, Rosen Y, Bistline J, Venkatesan K, Reddy A, Sonkin D, Liu M, Lehar J, Korn JM, Porter DA, Jones MD, Golji J, Caponigro G, Taylor JE, Dunning CM, Creech AL, Warren AC, McFarland JM, Zamanighomi M, Kauffmann A, Stransky N, Imielinski M, Maruvka YE, Cherniack AD, Tsherniak A, Vazquez F, Jaffe JD, Lane AA, Weinstock DM, Johannessen CM, Morrissey MP, Stegmeier F, Schlegel R, Hahn WC, Getz G, Mills GB, Boehm JS, Golub TR, Garraway LA, Sellers WR. Next-generation characterization of the Cancer Cell Line Encyclopedia. *Nature*. 2019;569(7757):503-508.
63. Gambardella G, Viscido G, Tumaini B, Isacchi A, Bosotti R, di Bernardo D. A single-cell analysis of breast cancer cell lines to study tumour heterogeneity and drug response. *Nat Commun*. 2022;13(1):1714.
64. Beckman RA, Schemmann GS, Yeang CH. Impact of genetic dynamics and single-cell heterogeneity on development of nonstandard personalized medicine strategies for cancer. *Proc Natl Acad Sci U S A*. 2012;109(36):14586-14591.
65. Yeang CH, Beckman RA. Long range personalized cancer treatment strategies incorporating evolutionary dynamics. *Biol Direct*. 2016;11(1):56.
66. Loeb LA, Kohrn BF, Loubet-Senear KJ, Dunn YJ, Ahn EH, O'Sullivan JN, Salk JJ, Bronner MP, Beckman RA. Extensive subclonal mutational diversity in human colorectal cancer and its significance. *Proc Natl Acad Sci U S A*. 2019;116(52):26863-26872.
67. Beckman RA, Loeb LA. Rare Mutations in Cancer Drug Resistance and Implications for Therapy. *Clin Pharmacol Ther*. 2020;108(3):437-439.
68. Ademuyiwa FO, Northfelt DW, O'Connor T, Levine E, Luo J, Tao Y, Hoog J, Laury ML, Summa T, Hammerschmidt T, Guo Z, Frith A, Weilbaecher K, Opyrchal M, Aft R, Clifton K, Suresh R, Bagegni N, Hagemann IS, Iglesia MD, Ma CX. A phase II study of palbociclib plus letrozole plus trastuzumab as neoadjuvant treatment for clinical stages II and III ER+ HER2+ breast cancer (PALTAN). *npj Breast Cancer*. 2023;9(1):1.
69. Ciruelos E, Villagrasa P, Pascual T, Oliveira M, Pernas S, Pare L, Escriva-de-Romani S, Manso L, Adamo B, Martinez E, Cortes J, Vazquez S, Perello A, Garau I, Mele M, Martinez N, Montano A, Bermejo B, Morales S, Echarri MJ, Vega E, Gonzalez-Farre B, Martinez D, Galvan P, Canes J, Nuciforo P, Gonzalez X, Prat A. Palbociclib and Trastuzumab in HER2-Positive Advanced Breast Cancer: Results from the Phase II SOLTI-1303 PATRICIA Trial. *Clin Cancer Res*. 2020;26(22):5820-5829.
70. Mahdi AF, Ashfield N, Conlon NT, Crown J, Collins DM. Abstract P3-07-16: Pre-clinical study of amcenestrant and HER2-targeted therapies in HER2+/ER+ breast cancer cell line models. *Cancer Research*. 2023;83(5_Supplement):P3-07.

825 71. Shagisultanova E, Crump LS, Borakove M, Hall JK, Rasti AR, Harrison BA, Kabos P,
826 Lyons TR, Borges VF. Triple Targeting of Breast Tumors Driven by Hormonal Receptors
827 and HER2. *Mol Cancer Ther*. 2022;21(1):48-57.
828 72. Madhavan S, Beckman RA, McCoy MD, Pishvaian MJ, Brody JR, Macklin P. Envisioning
829 the future of precision oncology trials. *Nat Cancer*. 2021;2(1):9-11.

830

## ADDITIONAL FILES

**Additional file 1:** Supplemental materials and methods. **Table S1.** List of primer sequences used for the detection of transcripts. Supplemental figures and figure legends: **Figure S1.** Effects of HER2- and ER-targeted therapies on ER expression and phosphorylation of HER2 in HER2+/ER+ LTEDs. **Figure S2.** Breast tumors harboring mutated genes identified in MM361 LTED cells are associated with HER2+ status and lower PR expression. **Figure S3.** Cluster analysis of MM361 parental and LTED cell scRNAseq data. **Figure S4.** scRNAseq expression of *ESR1* and *ERBB2* in MM361 parental and LTED cells. **Figure S5.** Ferroptosis-related genes in MM361 LTEDs. **Figure S6.** Dual targeting of HER2 and GPX4 increase cell death of BT474 LTEDs. **Figure S7.** Effects of TP and RSL3 on protein expression of ferroptosis lipid peroxidation markers (4-HNE and MDA).

**Additional file 2: Table S2.** Shared genes bearing exonic mutations in MM361 LTEDA and B versus parental cells and predicted pathogenicity.

**Additional file 3: Table S3.** Differentially expressed genes that are shared in the LTEDA and LTEDB variants of the MM361 cell line, and inference of transcriptional regulators using LISA (http://lisa.cistrome.org/, accessed on 4 May 2023).

## FIGURE LEGENDS

**Figure 1. Survival analysis for HER2+ BCa regarding their ER status. (A)** Compared to early-stage disease, five-year survival rates from the SEER database (https://seer.cancer.gov/statistics-network/explorer, accessed on 6 February 2023) are lowest for patients with late (distant)-stage HER2+ BCa subtype, regardless of their HR status. Error bars represent SEM. One-way ANOVA followed by Tukey's multiple comparison was performed to compare between groups; ***$p < 0.001$ denotes statistically significant. **(B-D)** Patients of the HER2+ BCa subtype expressing high levels of *ESR1* have a significantly lower probability for metastasis. Ten-year survival curves for HER2+ BCa patients stratified by high and low gene

857 expression of *ESR1* (205225_at). Plots were generated from KM Plotter database for BCa
858 (www.kmplot.com, accessed on 2 February 2023) and show hazard ratio (HR) at 95%
859 confidence, log-rank P values and number of patients (n). OS: Overall survival; RFS: Relapse-
860 free survival; DMFS: Distant metastasis-free survival.
861
862 **Figure 2. Growth pattern and response to ER- and HER2-targeted therapies of**
863 **HER2+/ER+ LTED variants differ from their parental counterparts. (A)** Western blot
864 validation that BT474 and MM361 express HER2 and ER. **(B)** Schematic illustrates our
865 preclinical modeling of ER-targeted therapy resistance by establishing two LTED variants (A
866 and B) for each of the BT474 and MM361 cell lines. **(C)** Growth curves for parental (BT474 and
867 MM361) and their LTED-derived (A and B) variants. Parental cells were cultured in either
868 normal growth media (IMEM supplemented with 10% FBS) or hormone-deprived media (phenol-
869 red free IMEM supplemented with 10% CSS). Parental cells of the CSS group were hormone-
870 deprived for 72 h before seeding. Plots represent mean ± SEM from two independent
871 experiments, each performed in triplicates and asterisks denote significant changes using one-
872 way ANOVA followed by Dunnett's multiple comparison test. **(D)** Parental MM361 is intrinsically
873 resistant to TP treatments whereas both MM361 and BT474 LTED models are less responsive
874 to ICI. Crystal violet growth assay after six days of treatments with either vehicle, 10 nM E2 + 1
875 μM ICI or 1 μg/ml T + 1 μg/ml P. Representative graph with data presented as mean ± SEM
876 from three independent experiments with six readings and analyzed by ANOVA using Dunnett's
877 multiple comparison test. *$p < 0.05$, **$p < 0.01$ and ***$p < 0.001$ were considered
878 statistically significant.
879
880 **Figure 3. Expression and genomic activity of ER is either preserved or lost in our**
881 **HER2+/ER+ LTED models. (A)** Western blot analysis show that ER protein is drastically
882 reduced in the MM361 LTED models but preserved in the BT474 LTEDs. **(B)** Blots from (A)

were analyzed by densitometry using ImageJ. Protein expressions were normalized to GAPDH and graphed as mean ± SEM from at least two independent experiments. ANOVA followed by Dunnett's multiple comparison test was performed to compare groups and statistical significance is shown on the graph. **(C-D)** Expression of *ESR1* and ER-target genes (*PGR* and *TFF1*) are maintained in BT474 LTEDs but drastically reduced in MM361 LTEDs. mRNA levels of ER and selected ER-target genes under basal conditions or after estrogen stimulation (with either 1 nM or 10 nM E2 for 72 h) were analyzed by qRT-PCR and data represented as mean ± SEM of fold changes in transcript expression from four independent experiments. Asterisks denote significant changes using ANOVA followed by Dunnett's multiple comparison test. *$p < 0.05$, **$p < 0.01$ and ***$p < 0.001$ were considered statistically significant.

**Figure 4. MM361 LTEDs gain basal-like, HER2-E intrinsic subtypes and harbor mutations in transcriptional and chromatin regulatory factors. (A)** UMAP plot of scRNAseq data grouped by predefined PAM50 intrinsic molecular subtypes. **(B)** Bar graph quantifies the distribution of intrinsic subtypes. **(C-F)** Characterizing MM361 LTED mutations using WGS. **(C)** Single base substitution (SBS) mutational signatures for the entire genome of MM361 LTEDs. **(D)** Venn diagram intersection showing shared mutated genes at their exonic regions of MM361 LTEDA and B versus parental cells. **(E)** Quantifying SBS for non-silent mutated genes at exonic regions. **(F)** Mutational effect predictions using Varmap (https://www.ebi.ac.uk/thornton-srv/databases/VarMap, accessed on 11 August 2022).

**Figure 5. Lipid metabolism pathways are upregulated in LTEDs of the MM361 cell line. (A)** Transcriptional profiling from scRNAseq at FDR<0.05 and log2 fold change ≤-0.5 and ≥0.5 identified 356 DEG between parental and LTEDA and 674 DEG between parental and LTEDB. **(B)** A total of 202 DEG are shared in both LTED lines vs. parental cells. Venn diagram intersections show 156 shared upregulated and 46 shared downregulated DEG in the MM361

LTEDs vs. parental. **(C)** qRT-PCR was used to confirm increased expression of selected upregulated genes identified from the scRNAseq transcriptomic profiling. Data presented as mean ± SEM of fold changes in expression of each gene (LTEDs relative to parental cells) from three independent experiments. Asterisks denote significant changes using ANOVA followed by Dunnett's multiple comparison test. **(D)** Top 20 enriched biological processes in MM361 LTEDs. Overlapped up- and down-regulated DEGs (from B) in MM361 LTEDs were analyzed by GSEA using the REACTOME gene set, with FDR q-values <0.05. Red- and blue-filled boxes highlight metabolic pathways. **(E)** UMAP plots for *ALOX15B* and *GPX4,* among the upregulated genes of the lipid metabolism pathway being enriched in the MM361 LTEDs.

**Figure 6. Dual targeting of HER2 and GPX4 increase cell death of MM361 LTEDs. (A)** Representative immunoblot of three independent experiments showing enhanced expression of GPX4 protein in MM361 LTEDs. **(B-D)** Cells treated with either vehicle, 1 μg/ml T + 1 μg/ml P, 1 μM RSL3 or a combination of both for 72 h then stained with Hoechst to monitor total cell number (blue nuclei), and Sytox green to monitor dead cells (green nuclei) as in panels B and C or analyzed by western blot analysis as in D. **(B-C)** Sytox staining experiments show that cotreatments of TP + RSL3 induce the highest cell death in MM361 LTEDs. **(B)** Cell death representative images and **(C)** quantifications from two independent experiments with at least ten fields analyzed for each and data presented as mean ± SEM of cell death percentages. Asterisks denote significant changes using one-way ANOVA followed by Tukey's multiple comparison test; *$p < 0.05$ and ***$p < 0.001$ were considered statistically significant. **(D)** Treatment effects on GPX4 and pAKT protein levels were assessed with western blot analysis. Immunoblots are a representation of two independent experiments.

# Unraveling Vulnerabilities in Endocrine Therapy-Resistant HER2+/ER+ Breast Cancer

**Figure 1.**

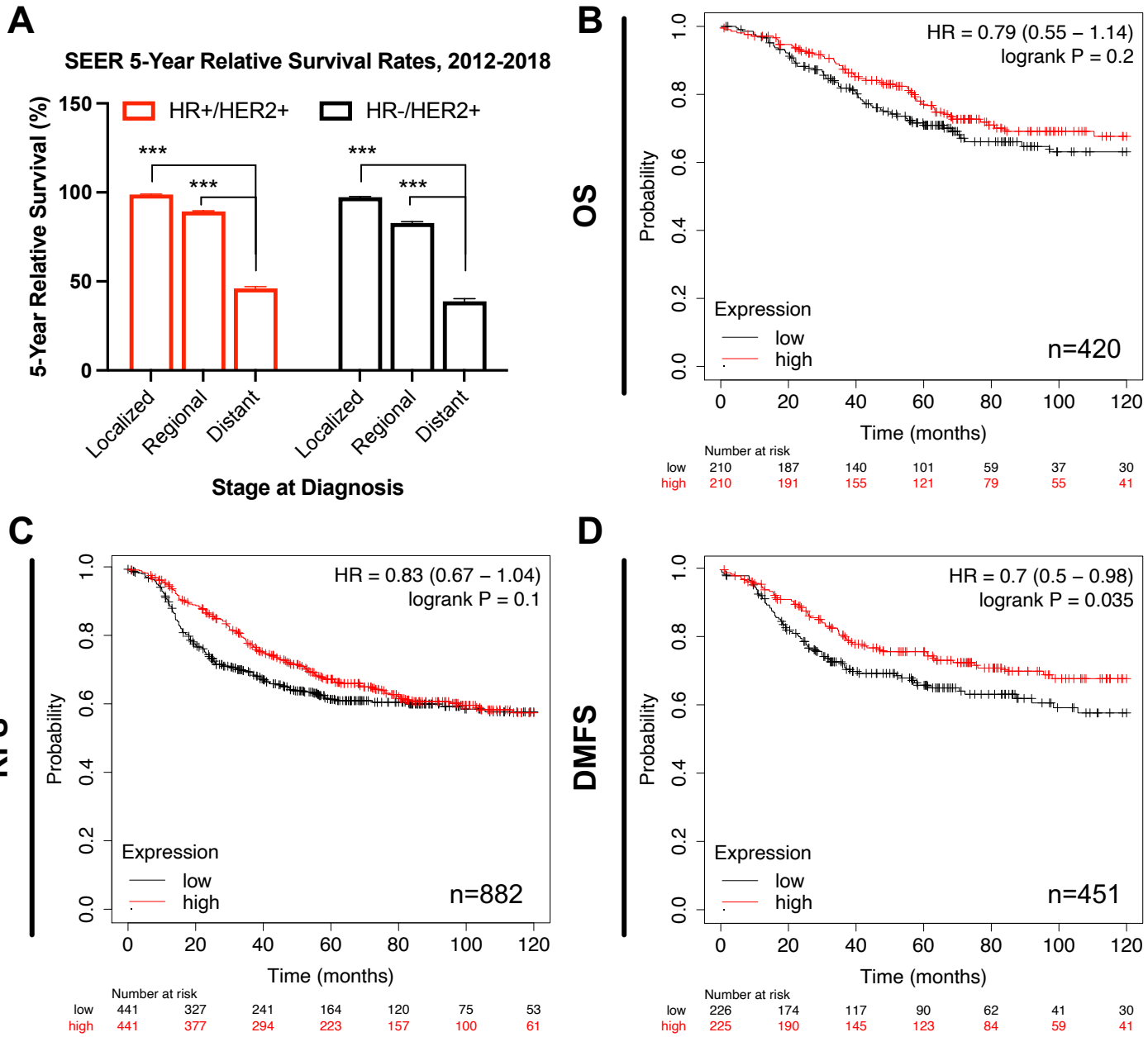

**Figure 2.**

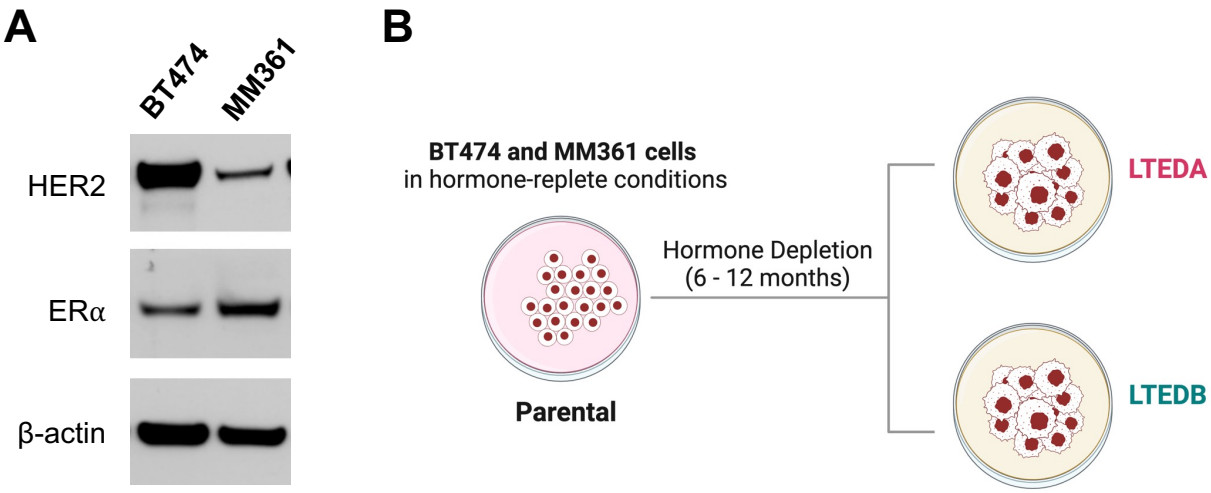


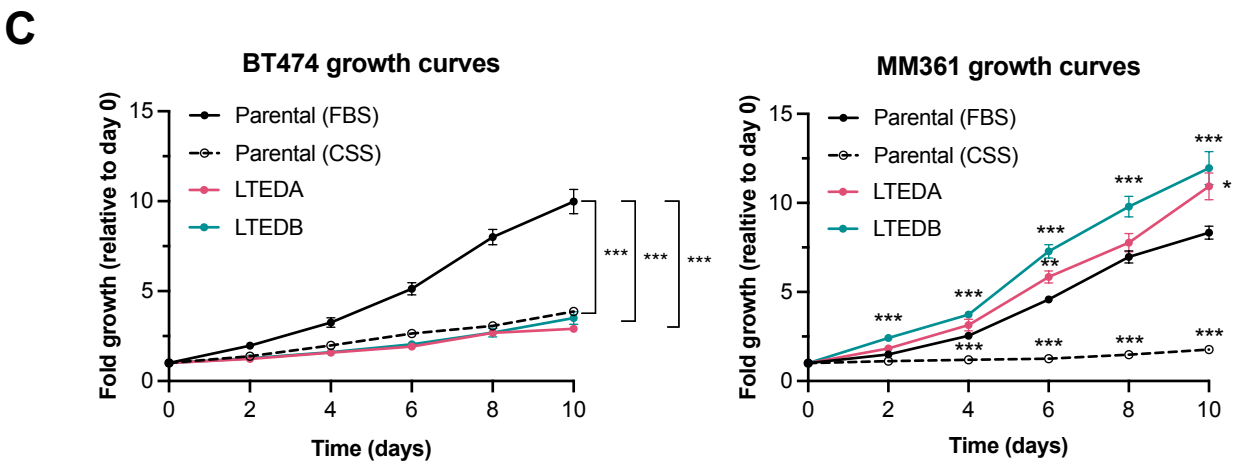


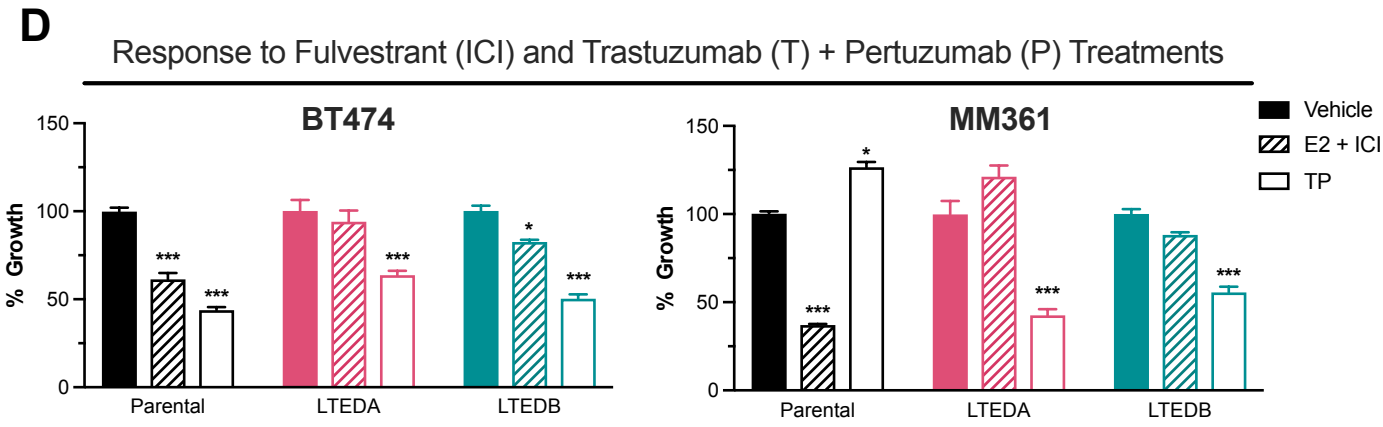

**Figure 3.**

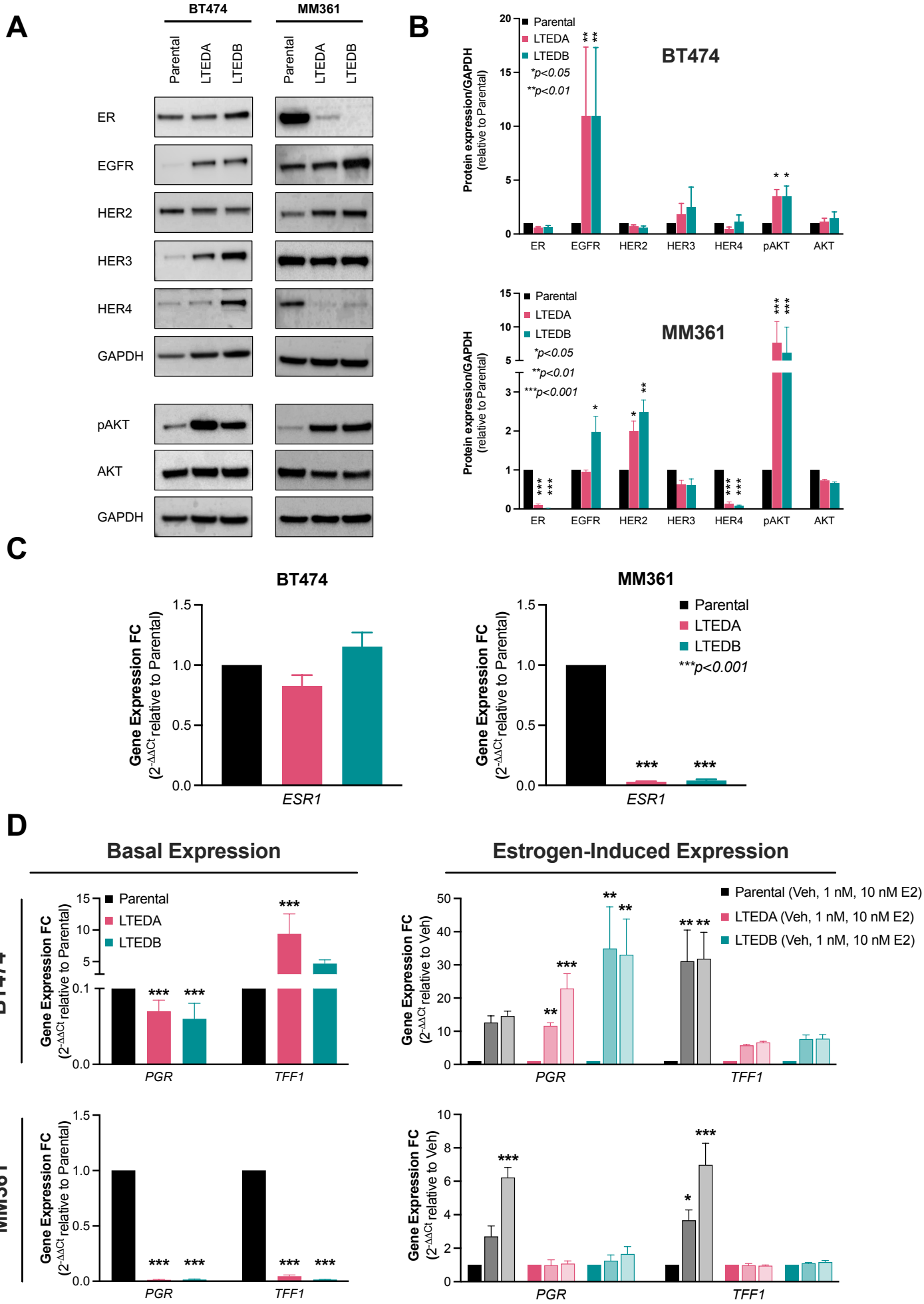

**Figure 4.**

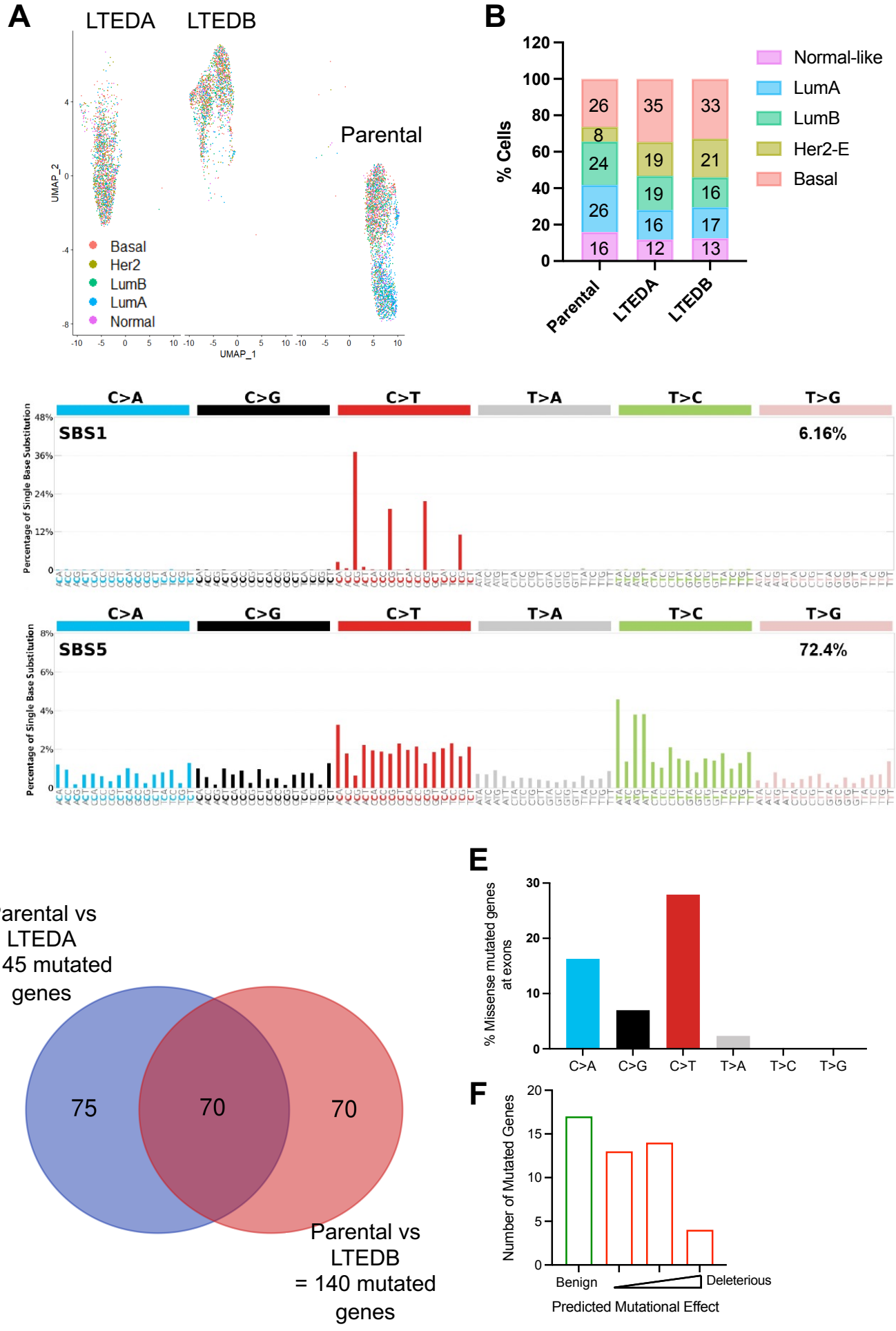

**Figure 5.**

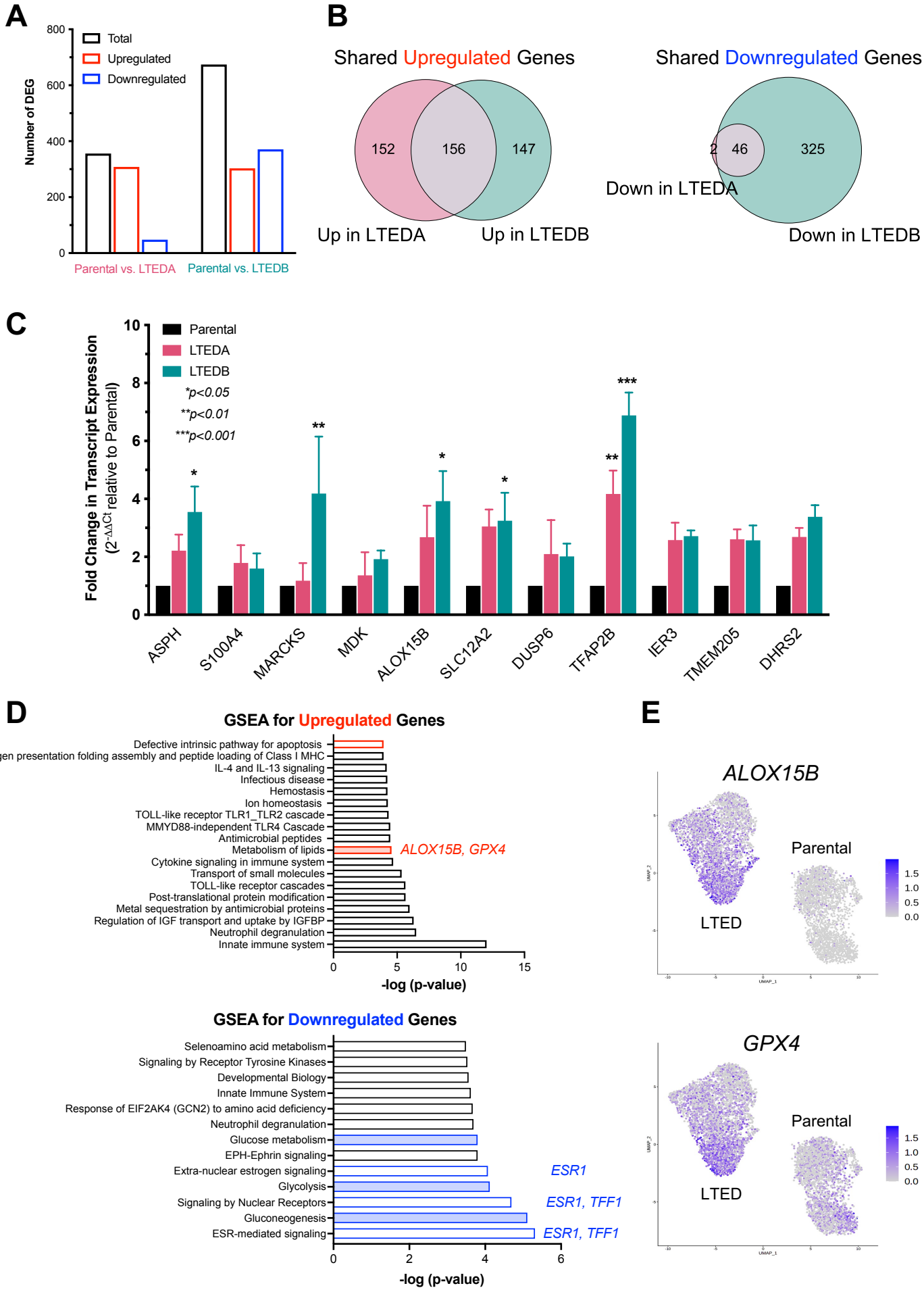

**Figure 6.**